

1 **A Novel Approach for Intra-Operative Shape Acquisition of the Tibio-Femoral**
2 **Joints Using 3D Laser Scanning in Computer Assisted Orthopaedic Surgery**

3 Shailesh V. Joshi, Philip J. Rowe

4 *Department of Biomedical Engineering, University of Strathclyde, Glasgow, G4 0TD, UK*

5 Primary email: joshi.shailesh87@gmail.com

6 Co-author email: philip.rowe@strath.ac.uk

7 **Address:** Department of Biomedical Engineering, University of Strathclyde, Wolfsan, 106
8 Rottenrow, Glasgow, G4 0TD, UK

9 **Telephone:** Dr Shailesh V Joshi: 07532058114

10 **Source of financial support:** This study was funded by International fees only studentship from
11 the University of Strathclyde.

12 **Category:** Original article

13 **Word count:** 5082; 6192 (including reference list)

14 **Number of figures:** 8

15 **Number of tables:** 3

16

17

Abstract

18

Background:

19

Image registration (IR) is an important process of developing a spatial relationship between pre-operative data and physical patient in the operation theatre. Current IR techniques for Computer Assisted Orthopaedic Surgery (CAOS) are time consuming and costly. There is a need to automate and accelerate this process.

20

21

22

23

Methods:

24

Bespoke quick, cost effective, contactless and automated 3D laser scanning techniques based on the DAVID Laserscanner method were designed. 10 cadaveric knee joints were intra-operatively laser scanned and were registered with the pre-operative MRI scans. The results are supported with a concurrent validity study.

25

26

27

28

Results:

29

The average absolute errors between scan models were systematically less than 1 mm. Errors on femoral surfaces were higher than tibial surfaces. Additionally, scans acquired through the large exposure produced higher errors than the smaller exposure.

30

31

32

33

Conclusion:

34

This study has provided proof of concept for a novel automated shape acquisition and registration technique for CAOS.

35

36

37

38

39 **Introduction**

40 Osteoarthritis (OA) is one of the most common musculoskeletal diseases affecting around
41 8.75 million of the population in UK¹. It is a chronic joint disorder characterised by degeneration
42 of the articular cartilage which results in a severe pain while performing daily voluntary
43 musculoskeletal activities. The knee joint is the most common site to be affected by OA and 4.7
44 million people in the UK had OA of knee in 2010. This is estimated to rise to 5.4 million by 2020¹.

45 After non-surgical treatments have been exhausted, patients suffering from OA of the knee
46 are usually advised to undergo knee replacement surgery where the articulating surfaces of the
47 tibio-femoral joint are resected and are replaced with prosthetic implants. Recently, knee
48 replacement surgery has been increasingly supported using the computers (Computer Assisted
49 Orthopaedic Surgery (CAOS)) along with advanced robotic systems. CAOS robotic procedures
50 such as MAKOpasty[®] typically comprise of three main phases: 1) Pre-operative planning; 2)
51 Intra-operative execution; and 3) Implant placement. Pre-operatively, high resolution DICOM
52 (Digital Imaging and Communications in Medicine) scans of the patient's knee joint are acquired
53 which are then used to plan the surgery. Based on this plan, intra-operatively the surgery is
54 performed with the help of computer navigation and robotics. Finally, the implant prosthesis is
55 precisely placed and its position is monitored with the navigation system.

56 In most CAOS applications for knee surgery, pre-operative CT scans are acquired on the
57 patient's leg and are segmented to create a patient specific 3D knee model. Image registration (IR)
58 is one of the important intra-operative phases of CAOS in which a spatial relationship between the
59 pre-operative imaging data and the physical patient present in the operation theatre is developed.
60 IR in most CAOS knee surgery applications is achieved using a manual method comprising hand-
61 held navigated probes. Anatomical points are acquired by physically touching the probe over the
62 articulating surfaces (tibial plateaux and femoral condyles) of the knee joint to form a point cloud

63 which can then be fitted to the pre-operative scan data using a best fit type minimisation. However,
64 this manual digitisation approach is laborious, time consuming and hence costly. In our recent
65 surgical trial of MAKOpasty^{®2} this process consumed upwards of 14-20 minutes³.

66 **Study Design**

67 In this study, a bespoke automated and contactless 3D laser scanner was built and used to
68 acquire the point clouds of the articulating surfaces of the cadaveric knee joints. In the first
69 concurrent validity, the laser and MRI scanned data of the cadaveric knee joints was compared to
70 establish the accuracy and reliability of the laser scanning technique.

71 In addition, a supplementary validity study was conducted for every cadaveric sample in
72 which the distance measurements acquired by the laser scanner were assessed against standard
73 digital vernier calliper measurements.

74 **Materials and Methods**

75 10 fresh frozen cadaver knee joints were used in the study. Eight out of the ten samples
76 were obtained from the Anatomy Gift Registry, 7522 Connelley Drive, Suite L, Hanover, MD
77 21076, USA. The remaining two samples were collected from the Clinical Anatomy Skills Centre
78 (CASC), Glasgow University, Glasgow, UK. All the samples were stored in the freezer at -19.5
79 °C and had their anatomical structure present from hemi-pelvis to toe.

80 Prior to these studies, all cadaver legs had been operated on post donation with a medial
81 UKA surgery. Lateral compartments of all the samples were intact with smooth articular cartilage
82 which were used in this investigation.

83

84

85

86 *Concurrent Validity Study 1:*

87 The surface topology of the cartilage surfaces was experimentally acquired using 3D
88 FLASH (Fast Low Angle Shot) MR imaging technique. This technique is used clinically and
89 provides high signal to noise ratio (SNR) and contrast to noise ratio (CNR) to adequately set apart
90 cartilage and bone interfaces in healthy as well as arthritic knee joints^{4, 5}. Although, 3D FLASH
91 MR imaging provides poor contrast between synovial fluid and cartilage and high sensitivity to
92 the artefacts; the technique still makes the segmentation of the articular cartilage and bone
93 relatively easier and is still therefore considered the standard MR imaging technique for depicting
94 articular cartilage morphology⁴⁻⁸.

95 All the samples were thawed 48 hours prior to the MR imaging and were scanned on a
96 Siemens MRI station at 1.5 T using 3D FLASH technique. A standard protocol presented in the
97 literature was followed^{4, 5, 9}. The slice thickness was 1 mm with no gap width. With a field of view
98 (FOV) of 160 mm, flip angle of 12° was set at 0.3 mm X 0.3 mm in plane resolution and 512 X
99 512 acquisition matrix. The protocol was approved by a highly skilled clinical imaging research
100 team in the Western Infirmary, Glasgow where the scanning was performed. A sagittal MRI was
101 performed (figure 1) and the scan slices were converted into a 3D volume. Samples were placed
102 in the freezer post MRI scanning.

103
104
105

Figure 1: A sample MRI scan of the right knee joint

106

107 DICOM MRI images were segmented using advanced clinical software Mimics
108 (Materialise's Interactive Medical Image Control System) designed for medical image processing.
109 3D point clouds of the articular cartilage surfaces were generated and were exported in binary.
110 STL (Stereolithography) format using the STL+ module.

111 For the laser scanning, a low cost range scanner was constructed using basic components such
112 as a calibration mask, a camera and a laser source¹⁰. Winkelbach and co-authors¹¹ provided a real-time
113 self-calibrating hand-held 3D laser scanning system, which is now also known as DAVID
114 Laserscanner. This system is free from markers and uses sub-pixel analysis of greyscale difference
115 images. This method works with a fast surface registration and with an improved random surface
116 matching process based on the RANSAC (Random Sample Consensus) algorithm¹². This approach is
117 not only robust and efficient but also can match frames of objects without the need for an initial guess
118 of the position.

119 Using the typical DAVID Laserscanner software package, scanning can be achieved with
120 satisfactory accuracy and precision; but, the calibration planes need to be placed behind the object
121 at all times during scanning. Due to the complexity in the knee joint and its positioning in the
122 theatre, keeping the calibration curves behind the knee during scanning would be highly
123 impractical. Moreover, hand-held scanning could be further time consuming due to irregularities
124 in the manual movement by human arm. However, more recent versions of the software enable users
125 to perform the scanning without calibration planes; provided that the laser source is moved in a precise
126 constant motion and the relative distance between the receiving camera and the laser source remains
127 fixed at all times. Thus, the scanner developed using DAVID Laserscanner was automated to
128 eliminate the use of calibration planes during actual scanning.

129 After an extensive review of the relevant literature, possible laser emitters of suitable
130 wavelength and power output were found which could generate a safe and undistorted output¹³⁻¹⁷.
131 A low cost (£3) class 2 line laser module (1 mW, 650 nm) was interfaced with a standard Logitech
132 720p detector webcam costing £17. The laser source was attached to the shaft of a geared bipolar
133 stepper motor using a bespoke machined T-joint slot. A2 sized calibrations planes were used for
134 the calibration and were then removed for the actual scanning.

135 The laser emitter (attached to the geared stepper) and the detector camera were mounted
136 on a robust positioner assembly constructed using Aluminium extrusion plates (figure 2 (a)). In

137 addition, the scanning modules were mounted on the end-effector of the MAKO Surgical Corps's
138 RIO® arm shown in the figure 2(b). This mimics the setup which would be possible if this robotic
139 surgical system was in use during MAKOplasty® surgery.

140

141 Figure 2: 3D Laser scanner (a): Scanner mounted on the aluminium extrusion framework (b):
142 Laser scanner mounted on the joint six of the MAKO RIO® arm

143

144 Each cadaveric leg sample was again thawed 48 hours prior to the experiments. The
145 samples were attached to a surgical table in a typical knee flexed operating position using straps
146 around the hemi-pelvis as shown in the figure 3. The foot was attached to a sliding foot holder to
147 allow variable knee flexion. The scans for each leg were acquired using two setups (Aluminium
148 extrusion and RIO) to investigate whether there is any difference between the bulky extrusion
149 based scanner and a more portable RIO mounted scanner. In addition, two typical surgical
150 exposures (UKA, TKA) were used as variables.

151

152 Figure 3: Sample cadaver set up on the bed with the attached arrays for MAKO registration

153

154 The laser scans were post processed using a robust digital image software package,
155 Geomagic Qualify®12. This software is certified and has received very high accuracy certification
156 from widely accepted organisations such as Physikalisch-Technische Bundesanstalt (PTB)
157 institute and National Institute of Standards and Technology (NIST) in the area of least squared
158 surface and curve fitting (Accurate up to 0.1 µm in length and 0.1" [1/36,000 of a degree] in
159 angle)¹⁸.

160 Each laser scan (test) was first visually aligned using manual registration with the
161 segmented MRI (reference) (figure 4) by selecting 3 to 9 common points on each surface. This is

162 a type of surface registration (point based registration or free-form surface matching) that works
163 closely on the Iterative Closet Point (ICP) algorithm where the two surfaces are aligned with
164 respect to the closest points leading to the segments and the triangles¹⁹⁻²¹. Thus, manual registration
165 adjusts spatial position of the floating scan using position of the fixed scan based on the user-
166 defined pairs of corresponding points from each scan.

167

168 Figure 4: Manual registration by selecting random points over the left lateral tibial surface

169 (a): MRI generated 3D model (red) of the articular cartilage, set as a reference model. (b):
170 Corresponding 3D laser scan (green) of the same cartilage acquired intra-operatively, set as a test
171 model. (c): Rough manual registration between two surfaces

172

173 After approximate manual registration, global registration was performed where the
174 alignment between the models is automatically fitted using ICP algorithm based on their spatial
175 position. Here, the fixed and floating scans are both moved around slightly to find the best
176 alignment possible. After this rough registration, reference and test models were aligned using ICP
177 based automatic best fit type of minimisation to produce a fine-tuned fit in order to evaluate
178 absolute errors between scans. In this alignment stage, test (laser) scan is sampled and the closest
179 points are computed to each point on the reference scan, based on the selected sample size. Using
180 the least-squares method, the sums of squares of distances between the sample pairs are evaluated
181 which are minimized over all the rigid motions that could realign the two objects. Having done
182 this, the closet points are re-computed on the reference to establish a new transformation matrix.
183 With the results of the fit, average absolute errors (AAE) between the models were calculated.
184 Each deviation is a Euclidean distance in a 3D space between the two closest points. 3D color-
185 coded mappings of residual differences between the scans were then generated to visualise the
186 spatial distribution of the errors.

187 In the experimental design, three independent variables were used each with two levels
188 viz., the exposure (UKA, TKA), the positioner setup (Aluminium assembly, MAKO RIO), and
189 type of the surface (tibia, femur). A Repeated measures ANOVA test was performed using a
190 standard statistical software package, SPSS (developed by IBM Corporation, NY, USA) to
191 investigate the effects of the independent variables on the dependent variable (AAE).

192

193 *Validity Study 2:*

194 At the end of the scanning session for each sample, cadaver legs were employed in the
195 subsequent validity study where the Euclidean distance measurements acquired using 3D laser
196 scanner were compared with the standard digital vernier callipers measurements. Tibial and
197 femoral articulating condyles were treated as separate surfaces thereby providing 20 set of
198 surfaces. On each surface, 7 M2 screws were inserted in a random pattern but with a good spread
199 as shown in figure 5(a). The distances between the centres of each screw with the centres of every
200 other screw were measured thus providing 21 different distance measurements on each surface as
201 shown in figure 5(b). The 21 measurements for each of the 20 surfaces resulted in $21 \times 20 = 420$
202 different measurements. For every surface, 10 laser scans were acquired. Thus, in total 4200
203 distance measurements acquired from laser scans were compared with the corresponding digital
204 vernier calliper measurements.

205

206 Figure 5: Distance measurements between the screw markers on the tibial condyle
207 (a): Placement of seven screws over the surface (b): Total number of measurements (21)
208 computed between every pair of the points (c): Direct distance measurement acquired using
209 digital vernier calliper (d): Distance measurement (in the white box) acquired on the
210 corresponding digitised 3D laser scan and formulated using Geomagic Qualify[®]

211

212 The laser scans were analysed in Geomagic Qualify® 12 in which the distances between
213 the pairs of screws were evaluated using the distance calculation tool based on the Euclidean
214 metric calculation in the 3D space (figure 5(d)).

215 For every set of measurements, an absolute error (AE) and absolute percent error (APE)
216 were computed followed by average absolute error (AAE) and average absolute percentage error
217 (AAPE, also known as MAPE, mean absolute percentage error). Significance in both studies was
218 tested at $\alpha=0.05$ level.

219 **Results**

220 The key findings of the studies are reported in this paper. The in-depth investigation is
221 available online¹⁰. The outcome of the data comparison for a single femoral scan example is
222 explained in detail with its deviation distribution and spatial distribution of the deviations in a
223 colour coded pattern. This is followed by a summary table of all the samples.

224 This particular example (figure 6 and 7) shows a comparison between MRI and the laser
225 scan of the right femoral lateral cartilage. The AAE* of 0.21 mm was reported with SD_{AE}^* of 0.32
226 mm. The $+d_{max}^*$ and $-d_{max}^*$ were 1.88 mm and -1.38 mm respectively.

227

228 Figure 6: Deviation distribution between MRI and laser scan of an example right femoral lateral
229 cartilage

230 Deviation in mm is plotted against the percentage of points within the range of deviations. Note:
231 $\pm d_{max}$ occurred at the periphery

232

233

* AAE: Average absolute error, SD_{AE} : Standard deviation of the absolute error, $+d_{max}$: Maximum positive deviation, $-d_{max}$: Maximum negative deviation

234 Figure 7: Top view of the colour deviation map showing spatial distribution of the deviations
235 between MRI and laser scan of right femoral lateral cartilage

236 The posterior and superior condylar region is clipped as the laser scan was acquired with a
237 minimal exposure (90 mm, mimicking UKA). Note: Large errors ($\pm d_{\max}$) at the periphery of the
238 scan

239

240

241

242

243 Table 1: Summary of the alignment statistics between MRI and laser scans of
244 femoral surfaces of all the samples

245 AAE; average absolute error between the models, SD_{AE} ; standard deviation of the absolute error,
246 $+d_{\max}$ and $-d_{\max}$; maximum positive and negative deviations respectively. Average and standard
247 deviation of all the parameters is shown at the bottom of the table. Note: d_{\max} values occurred at
248 the periphery of the scan zones

249

250

251

252

253

254 Table 2: Summary of the effects of the independent variables on AAE between MRI and laser scans

255

256 The main and interaction effects of the independent variables indicating the P-value statistics, the
257 significance of the statistics and the interpretation of the results

258

259

260

261

262

263

264

265

Effects of independent variables:

266 In the next stage, the effects of three independent variables i.e. type of setup (Aluminium
267 extrusion, RIO), type of exposure (UKA, TKA) and type of surface (Tibia, Femur) on the
268 dependent variable, AAE were studied. The main effects of the independent variables as well as
269 the interactions between the variables were studied. The summary of this analysis is reported in
270 table 2.

271

272 *Validity Study*

273 A bar graph (figure 8(a) and 8(b)) along with error bars depicting variations in the
274 measurements is shown for one of the 20 surfaces. In addition, a summary of all the 4200
275 measurement comparisons is reported in table 3. Both the methods (laser and vernier calliper) were
276 responsive so changing the differences between the screws and inter measurement system
277 differences were small with 95% of the scanned measurements within 1 mm of the vernier
278 callipers.

279

280 Figure 8: Bar graph comparison for the distance calculations between vernier calliper and 3D
281 laser scans

282 (a): Bar graph for first 11 pairs of screws. (b): Bar graph for remaining 10 pairs of screws

283 Note: Blue bar is the measurement recorded by the vernier calliper, whereas red bar is the mean
284 value of the measurements on the laser scans. Error bars indicate the range of values (minimum
285 and maximum values). All the measurement differences between vernier calliper and laser were
286 statistically not significant; $P > 0.05$

287

288 Table 3: Summary of the assessment of the distance calculations performed using direct
289 measurements (vernier calliper) and the 3D laser scans

290 AAE; average absolute error between measurements, SD_{AE} ; standard deviation of the absolute
291 error, AAPE; average absolute percentage error, SD_{APE} ; standard deviation of the absolute
292 percentage error. Average and standard deviation of all the parameters is shown at the bottom of
293 the table. Note: NS= Not significant. All the measurement differences between vernier calliper
294 and laser were statistically not significant; $P > 0.05$

295

296 **Discussion**

297 Over the last decade, CAOS has emerged particularly in the area of minimally invasive
298 UKA surgery. With the more conservative approach of UKA (as compared to TKA), which have
299 been reenergised with the development of the advanced robotic systems, only the affected

300 compartment (medial/lateral) is resected and an implant is placed to facilitate normal joint
301 function. One of the most important phases of the computer assisted surgical process in the
302 operating theatre is to develop a spatial relationship between the pre-operatively acquired patient
303 specific scan of the knee surface and the physical patient knee present in the operating theatre. It
304 is possible to visualise key anatomical points around the patient's knee joint in the CT/MRI scan
305 as well as to locate the same points on the actual patient during surgery using intra-operative
306 sensors or probes. However, their spatial correspondence remains unknown until IR is achieved.
307 IR is the process that generates the relationship between the scan and the patient and allows the
308 surgeon to visualise the 3D pre-operative scan data in-relation to the patient's anatomy in the
309 operating theatre. It is therefore a crucial aspect of the procedure. This study demonstrates a novel
310 laser scanning technique which is proposed as an alternative to the current time consuming IR
311 methods in knee CAOS. Laser based registration can be achieved in less than half the time used
312 in the manual technique which can save time in the theatre and thus cost⁴¹.

313 An example showing detailed comparison between MRI and corresponding laser scan of
314 the cadaveric femoral condyle has been presented (figure 6 and 7). The average deviation (AAE)
315 between the laser and MRI scans was 0.32 mm with a standard deviation (SD_{AE}) of 0.32 mm. The
316 maximum positive ($+d_{max}$) and negative ($-d_{max}$) deviations were +1.88 mm and -1.38 mm
317 respectively. The total number of point pairs used for the data comparison was 5266 out of which
318 98.48% were within ± 0.94 mm of deviation. Moreover, in figure 7, it can be clearly seen that the
319 absolute errors tend to increase as the extreme edges of the scan area are approached. The tibial
320 surfaces and rest of the femoral surfaces showed a similar trend with maximum % of deviations
321 within ± 1 mm and higher errors towards peripheries. Summary of the alignment statistics between
322 MRI and laser scans of femoral surfaces for all the samples is shown in table 1.

323 The effects of independent variables (setup, exposure and surface) were investigated using
324 repeated measures ANOVA and are shown in table 2. There was no statistically significant

325 difference on AAE within two types of setups (Al and RIO), $F(1,9) = 1.148$; $P=0.312$ which
326 indicates that the bulky Aluminium extrusion setup can be replaced with the positioning RIO arm
327 which in our case would be already present in the theatre. Thus, it would be possible to make one
328 compact system consisting of the robot and the scanner and save plenty of space in the operating
329 theatre. The AAE with TKA exposure was significantly higher than UKA exposure, $F(1,9) =$
330 40.808 ; $P= 0.0001$. It may seem that greater errors occurred with greater exposure but this was a
331 result of exposing more edges to the scan where the surface was at a greater angle to the incident
332 laser light and hence, the errors in depth perception possibly produced larger errors between the
333 laser scan and the MRI images. However, these errors remained sub-millimetric. The AAE on the
334 femoral surfaces was significantly higher than on the tibial surfaces, $F(1,9) = 14.863$; $P = 0.004$.
335 The ends of the femoral condyles contain more regions where the profile of the bone surface is at
336 a greater angle to the incident laser light and hence higher errors at the peripheries contribute to
337 overall higher AAE. However, these errors were again sub-millimetric. In other words, the higher
338 errors with TKA exposure (as compared with UKA exposure) and on femoral surfaces (as
339 compared to tibial surfaces) can be attributed to the ‘edge effect’ which affects most triangulation
340 systems. It can be seen in the colour coded deviation distribution map (figure 7) where the higher
341 % of the larger deviations appeared on the peripheries. 3D scanners and particularly laser based
342 scanners tend to produce errors at the spatial discontinuities or edges of the surfaces being scanned.
343 When the laser hits the surface edges, only a certain part is reflected from the actual point and
344 some reflection is always induced by the adjacent surfaces or the surface behind the object. Thus,
345 the final signal is a mixture of the signals from the foreground and the background. This
346 phenomenon is called a ‘mixed-pixel effect’ or ‘edge effect’. Due to the higher slope on the edge
347 of the surface and the viewing direction of the scanner, the laser plane falls almost tangentially on
348 the edge which leads to errors in location of these points in the cloud and thus causes inaccuracies
349 and distortions in the scan²²⁻²⁸.

350 During the scanning, the scanner was always positioned such that the surface (tibial and
351 femoral condyle) being scanned was in the centre of the camera image. With the TKA incision,
352 additional surface exposure is provided which is usually towards the peripheral region of the
353 surface. Also, femoral condyles are more non-uniform and curved in their surface topography
354 when compared to the tibial plateau. So, while scanning the femoral condyles, there is a higher
355 slope of the target around the edges and the curved region which causes higher deviations in those
356 areas. As a result, the laser plane incidents more tangentially on the femoral condyles as compared
357 to the tibial plateau and thus the edge effect results in higher deviations.

358 Furthermore, a careful statistical investigation showed that there was no significant
359 interaction (two-way and three-way) found between the variables. As the interactions were not
360 significant, the main effects of the independent variables can be accepted²⁹⁻³².

361 The second stage in the experimental design was to compare the automated distance
362 measurements acquired using the developed laser scanner with the manual measurements from
363 digital vernier calliper, an approach widely accepted in research and industry to evaluate the
364 technical performance of 3D imaging system for geometric accuracy³³⁻⁴⁰. A bar graph with error
365 bars for an example surface is presented in figures 8(a) and 8(b). The rest of the surfaces followed
366 a similar pattern. The error bars indicate the range (minimum and maximum) of the reported
367 values. The AAE values ranged from 0.3 mm to 0.62 mm with a mean of 0.46 mm and SD of 0.08
368 mm. The SD_{AE} within each surface was 0.15 mm. Furthermore, for every set of data, AAPE was
369 reported which ranged from 1.19% to 2.45% with the mean of 1.66% and SD of 0.31%. The mean
370 standard deviation of AAPE within each surface (SD_{AAPE}) was 0.82% with SD of 0.24% and
371 min/max values of 0.54% and 1.40%. The measurements between two systems were analysed
372 using two sample independent t-test³⁵. The P-values for each surface comparison are reported in
373 table 3. None of the differences were statistically significant, $P > 0.05$ and in fact the P-values were
374 very close to 1. Hence, we conclude that there is no sufficient evidence to suggest that laser

375 readings and vernier calliper distance measurements were different. The mean of the deviations
376 (Mean AAE) for all the 20 surfaces was less than 0.5 mm (0.46 mm) with an average SD_{AE} of 0.15
377 implying that 95% of the deviations (4200 measurements) lay within 0.46 ± 0.3 (2 SD) i.e. within
378 0.16-0.76 mm absolute deviation which is suitable for orthopaedic surgeries.

379 *Limitations and future recommendations*

380 3D laser scanners have obvious advantages such as high speed, accuracy, precision and
381 reproducibility. However, their strength can be affected by various factors. Stray light or an
382 unidentified light source can affect the quality of the scans. Thus, care must be taken to avoid such
383 sources and most importantly any proximal light source which might enter the triangulation plane
384 i.e. the plane formed by camera, laser source and object being scanned. Shadow of the surrounding
385 structures can produce gaps in the scans. Due to the awkward and complex structure of the tibio-
386 femoral joint, femoral condyles may produce occultation on tibial plateaux. Further safely flexing
387 the knee joint can enable the user to acquire maximum exposed area. Also, to avoid possible
388 hindrance, the skin surrounding the incision needs to be retracted, especially in the smaller UKA
389 exposures to allow the detector camera to completely visualise the area (condyles) under scrutiny.

390 A simple way of controlling the edge effect would be by removing any regions where the
391 slope of the scan is at an acute angle to the scanner as these are the areas that are most likely to
392 add higher magnitude of errors to the fitting. An automated process is thus required as manually
393 removing the edges would add additional time in the data post-processing phase in theatre. For the
394 validity study, inter-operator variation was eliminated but intra-operator variation should be
395 investigated by repeating the same measurement of the digital vernier calliper acquired by the
396 same operator to check the variation.

397 This project focussed on acquiring accurate 3D surface geometry of tibio-femoral joints in
398 the theatre. Optically navigating the scanner in real time was beyond the scope of this project.
399 However, as the next stage of the project, the laser line could be navigated using geometrical

400 principles and with use of marker frame which are tracked by the IR cameras already utilised in
401 the surgery. Once this is achieved, it could be possible to plan and execute the surgery in theatre
402 there and then. This imageless navigation would be very effective in terms of reduced cost, time
403 and radiation dosage and would provide convenience to patients and clinicians. The proof of
404 concept in real surgery is still to be obtained and is the next step in the process towards a suitable
405 medical device which can be used in the general surgery.

406 Commercially available high precision laser lines and high-speed CMOS wireless cameras
407 could be used instead of the scanning components used in the study and would further improve
408 the accuracy of the scans and reduce the acquisition time. Further scanning of more cadaver legs
409 should be undertaken and more independent variables should be explored such as distance between
410 centre of the scanner and surface being scanned, sex of the patient, cross sectional area of the
411 surface, etc.

412 **Conclusion**

413 A series of experiments in this study demonstrated that average deviations between the
414 MRI and the 3D laser scans were in general less than half a millimetre. This suggests that the
415 system can repeatedly acquire accurate 3D scans of the tibio-femoral cartilage and bone and in-
416 situ in the operating theatre environment. The second validity study has proven that the developed
417 laser scanner measurements were accurate, precise and repeatable as compared to the standard
418 measurement system such as digital vernier calliper. The sample size of 10 surfaces should be born
419 in mind with the sub-millimetric accuracy of the scans.

420 This study has addressed an important issue of replacing the current manual intra-operative
421 surface acquisition and image registration process of CAOS with 3D laser scanning. In this study,
422 the feasibility of using an automated 3D scanner based on the DAVID laser scanning technique
423 was validated. The system is capable of acquiring scans of the tibio-femoral joints in theatre to

424 generate complete 3D models of the surface geometry and to an accuracy less than 1 degree across
425 the whole scan surface. The proposed technique is completely contactless and does not require
426 critical points in the hidden regions of the joint thereby allowing surgeons to control the overall
427 incision size limited to the surface being burred. The system was built using inexpensive
428 components and the total cost of the scanning hardware was less than £200. Using the MAKO
429 Surgical registration approach to register each bone surface required approximately 15 minutes
430 whereas the overall time for proposed laser based registration was less than 4 minutes for every
431 joint out of which majority of the time was spent in the post processing of scans which could
432 further be automated.

433 The system and method have much to offer to CAOS in terms of speed and accuracy of
434 registration and also the potential for both imageless surgery as well as cartilage property
435 assessments.

436

437 **Acknowledgements**

438 We would like to thank Dr. Philip Riches for arranging the samples and the lab space as
439 well as providing assistance in acquiring the ethical approvals for the experiments. We are thankful
440 to Dr. Gareth Pierce for allowing us to perform pilot studies using the departmental laser scanner.
441 We would also like to thank to the research radiology team of the Western Infirmary, Glasgow for
442 the clinical scanning of the samples.

443

444 **Competing interests**

445 The authors have no competing interests to disclose.

446

447

Table 1: Summary of the alignment statistics between MRI and laser scans of femoral surfaces of all the samples

AAE; average absolute error between the models, SD_{AE} ; standard deviation of the absolute error, $+d_{max}$ and $-d_{max}$; maximum positive and negative deviations respectively. Average and standard deviation of all the parameters is shown at the bottom of the table. Note: d_{max} values occurred at the periphery of the scan zones.

Samples	UKA Exposure						TKA Exposure					
	On AI Extrusion			On RIO			On AI Extrusion			On RIO		
	AAE (mm)	SD_{AE} (mm)	d_{max} (mm)	AAE (mm)	SD_{AE} (mm)	d_{max} (mm)	AAE (mm)	SD_{AE} (mm)	d_{max} (mm)	AAE (mm)	SD_{AE} (mm)	d_{max} (mm)
1	0.23	0.33	1.84 -1.50	0.26	0.42	1.51 -1.67	0.28	0.42	1.81 -1.82	0.27	0.44	1.85 -1.94
2	0.20	0.29	2.07 -1.37	0.18	0.28	1.30 -2.03	0.35	0.68	2.15 -2.47	0.33	0.61	2.30 -2.24
3	0.28	0.40	1.49 -1.60	0.28	0.44	1.51 -1.86	0.33	0.46	1.49 -1.69	0.32	0.47	1.87 -1.89
4	0.23	0.33	1.84 -1.50	0.26	0.42	1.51 -1.67	0.28	0.42	1.81 -1.82	0.27	0.44	1.85 -1.94
5	0.21	0.28	1.15 -0.99	0.24	0.33	1.34 -1.31	0.25	0.46	2.73 -2.20	0.27	0.37	2.72 -1.97
6	0.25	0.58	1.43 -1.91	0.25	0.53	1.79 -1.88	0.29	0.66	2.53 -2.20	0.30	0.60	2.46 -2.54
7	0.21	0.31	1.75 -1.39	0.23	0.33	1.72 -1.37	0.28	0.32	1.74 -1.25	0.29	0.38	2.52 -1.46
8	0.26	0.44	1.36 -1.97	0.26	0.46	1.32 -2.19	0.28	0.59	1.97 -3.03	0.30	0.64	2.56 -2.46
9	0.29	0.38	1.23 -1.57	0.28	0.40	1.43 -1.56	0.32	0.45	1.63 -1.73	0.33	0.54	1.93 -2.32
10	0.24	0.36	1.66 -1.65	0.23	0.31	1.31 -1.13	0.30	0.40	2.18 -1.63	0.27	0.40	2.61 -2.50
Average	0.24	0.37	1.58 -1.55	0.25	0.39	1.47 -1.67	0.29	0.48	2.00 -1.98	0.29	0.49	2.27 -2.12
SD	0.03	0.09	0.30 0.28	0.03	0.08	0.17 0.33	0.03	0.12	0.39 0.51	0.03	0.10	0.35 0.35

Table 2: Summary of the effects of the independent variables on AAE between MRI and laser scans

The main and interaction effects of the independent variables indicating the P-value statistics, the significance of the statistics and the interpretation of the results.

Effects	Independent variables	P-value statistics	Significance	Interpretation
Main Effects	Type of Setup (AI, RIO)	$F(1,9) = 1.148$; $P = 0.312$	Not significant	No difference in two types of setup
	Type of Exposure (UKA, TKA)	$F(1,9) = 40.808$; $P = 0.0001$	Significant	Errors slightly larger with TKA exposure
	Type of Surface (Tibia, Femur)	$F(1,9) = 14.863$; $P = 0.004$	Significant	Errors slightly larger on femoral surface
Interaction Effects	Seup*Exposure	$F(1,9) = 0.13$; $P = 0.911$	Not significant	No interaction between setup and exposure
	Setup*Surface	$F(1,9) = 0.474$; $P = 0.509$	Not significant	No interaction between setup and surface
	Exposure*Surface	$F(1,9) = 1.097$; $P = 0.322$	Not significant	No interaction between exposure and surface
	Setup*Exposure*Surface	$F(1,9) = 0.682$; $P = 0.430$	Not significant	No interaction between setup, exposure and surface

454 Table 3: Summary of the assessment of the distance calculations performed using direct
 455 measurements (vernier calliper) and the 3D laser scans
 456 AAE; average absolute error between measurements, SD_{AE} ; standard deviation of the absolute
 457 error, AAPE; average absolute percentage error, SD_{APE} ; standard deviation of the absolute
 458 percentage error. Average and standard deviation of all the parameters is shown at the bottom of
 459 the table. Note: NS= Not significant. All the measurement differences between vernier calliper
 460 and laser were statistically not significant; $P > 0.05$
 461

Surface	AAE (mm)	SD_{AE}	AAPE (%)	SD_{APE}	P-value	Significance
1	0.49	0.17	1.66	0.65	0.930	NS
2	0.61	0.23	2.45	1.40	0.923	NS
3	0.44	0.12	1.66	0.91	0.972	NS
4	0.43	0.14	1.88	1.00	0.987	NS
5	0.48	0.13	1.72	0.63	0.993	NS
6	0.41	0.09	1.49	0.73	0.999	NS
7	0.38	0.13	1.47	0.76	0.992	NS
8	0.47	0.17	1.47	0.62	0.934	NS
9	0.50	0.12	1.55	0.67	0.996	NS
10	0.46	0.11	1.37	0.54	0.993	NS
11	0.49	0.12	1.88	0.80	0.967	NS
12	0.62	0.27	2.17	1.34	0.966	NS
13	0.59	0.23	2.18	0.97	0.986	NS
14	0.47	0.14	1.70	0.82	0.964	NS
15	0.43	0.20	1.50	0.65	0.976	NS
16	0.49	0.25	1.51	0.81	0.965	NS
17	0.39	0.14	1.49	1.10	0.978	NS
18	0.38	0.08	1.40	0.64	0.991	NS
19	0.30	0.09	1.19	0.70	0.974	NS
20	0.43	0.13	1.54	0.67	0.954	NS
Mean	0.46	0.15	1.66	0.82		
SD	0.08	0.05	0.31	0.24		

462

463 **Figure legends:**

464 Figure 1: A sample MRI scan of the right knee joint

465

466 Figure 2: 3D Laser scanner (a): Scanner mounted on the aluminium extrusion framework (b):
467 Laser scanner mounted on the joint six of the MAKO RIO[®] arm

468

469 Figure 3: Sample cadaver set up on the bed with the attached arrays for MAKO registration

470

471 Figure 4: Manual registration by selecting random points over the left lateral tibial surface

472 (a): MRI generated 3D model (red) of the articular cartilage, set as a reference model. (b):
473 Corresponding 3D laser scan (green) of the same cartilage acquired intra-operatively, set as a test
474 model. (c): Rough manual registration between two surfaces

475

476 Figure 5: Distance measurements between the screw markers on the tibial condyle
477 (a): Placement of seven screws over the surface (b): Total number of measurements (21)
478 computed between every pair of the points (c): Direct distance measurement acquired using
479 digital vernier calliper (d): Distance measurement (in the white box) acquired on the
480 corresponding digitised 3D laser scan and formulated using Geomagic Qualify[®]

481

482 Figure 6: Deviation distribution between MRI and laser scan of an example right femoral lateral
483 cartilage

484 Deviation in mm is plotted against the percentage of points within the range of deviations. Note:
485 $\pm d_{\max}$ occurred at the periphery

486

487 Figure 7: Top view of the colour deviation map showing spatial distribution of the deviations
488 between MRI and laser scan of right femoral lateral cartilage

489 The posterior and superior condylar region is clipped as the laser scan was acquired with a
490 minimal exposure (90 mm, mimicking UKA). Note: Large errors ($\pm d_{\max}$) at the periphery

491

492
493 Figure 8: Bar graph for the comparison for the distance calculations between vernier calliper and
494 3D laser scans
495 (a): Bar graph for first 11 pairs of screws. (b): Bar graph for remaining 10 pairs of screws
496 Note: Blue bar is the measurement recorded by the vernier calliper, whereas red bar is the mean
497 value of the measurements on the laser scans. Error bars indicate the range of values (minimum
498 and maximum values). All the measurement differences between vernier calliper and laser were
499 statistically not significant; $P > 0.05$

500

501 **References**

- 502
503 1. UK Ar. Osteoarthritis in General Practice Data and Perspectives 2013 [cited 2015 5
504 January]. Available from: [http://www.arthritisresearchuk.org/arthritis-information/data-and-](http://www.arthritisresearchuk.org/arthritis-information/data-and-statistics/osteoarthritis.aspx)
505 [statistics/osteoarthritis.aspx](http://www.arthritisresearchuk.org/arthritis-information/data-and-statistics/osteoarthritis.aspx)
- 506 2. Jones B, Blyth M, MacLean A, Anthony A, Rowe P, editors. Accuracy of UKA implant
507 positioning and early clinical outcomes in a RCT comparing Robotic Assisted and Manual
508 Surgery. CAOS; 2013. Orlando.
- 509 3. Banger M, Rowe P, Blyth M. Time analysis of MAKO RIO UKA procedures in
510 comparison with the oxford UKA. Bone & Joint Journal Orthopaedic Proceedings Supplement.
511 2013;95(SUPP 28):89-.
- 512 4. Kornaat PR, Reeder SB, Koo S, Brittain JH, Yu H, Andriacchi TP, et al. MR imaging of
513 articular cartilage at 1.5T and 3.0T: comparison of SPGR and SSFP sequences. Osteoarthritis and
514 cartilage / OARS, Osteoarthritis Research Society. 2005;13(4):338-44.
- 515 5. Eckstein F, Cicuttini F, Raynauld JP, Waterton JC, Peterfy C. Magnetic resonance imaging
516 (MRI) of articular cartilage in knee osteoarthritis (OA): morphological assessment. Osteoarthritis
517 and cartilage / OARS, Osteoarthritis Research Society. 2006;14 Suppl A:A46-75.
- 518 6. Recht M, Kramer J, Marcelis S, Pathria M, Trudell D, Haghghi P, et al. Abnormalities of
519 articular cartilage in the knee: analysis of available MR techniques. Radiology. 1993;187(2):473-
520 478.
- 521 7. Eckstein F, Charles HC, Buck RJ, Kraus VB, Remmers AE, Hudelmaier M, et al. Accuracy
522 and precision of quantitative assessment of cartilage morphology by magnetic resonance imaging
523 at 3.0T. Arthritis and rheumatism. 2005;52(10):3132-6.
- 524 8. Roemer FW, Crema MD, Trattinig S, Guermazi A. Advances in Imaging of Osteoarthritis
525 and Cartilage. Radiology. 2011;260(2):332-54.

- 526 9. Stahl R, Krug R, Kelley DA, Zuo J, Ma CB, Majumdar S, et al. Assessment of cartilage-
527 dedicated sequences at ultra-high-field MRI: comparison of imaging performance and diagnostic
528 confidence between 3.0 and 7.0 T with respect to osteoarthritis-induced changes at the knee joint.
529 *Skeletal radiology*. 2009;38(8):771-83.
- 530 10. Joshi S. Intra-Operative Shape Acquisition of Tibio-Femoral Joints Using 3D Laser
531 Scanning for Computer Assisted Orthopaedic Surgery: A Proof of Concept (Thesis). Glasgow:
532 University of Strathclyde; 2015.
- 533 11. Winkelbach S, Molkenstruck S, Wahl F. Low-Cost Laser Range Scanner and Fast Surface
534 Registration Approach. In: Franke K, Müller K-R, Nickolay B, Schäfer R, editors. *Pattern*
535 *Recognition*. Lecture Notes in Computer Science. 4174: Springer Berlin Heidelberg; 2006. p. 718-
536 28.
- 537 12. Fischler MA, Bolles RC. Random sample consensus: a paradigm for model fitting with
538 applications to image analysis and automated cartography. *Commun ACM*. 1981;24(6):381-95.
- 539 13. Marmulla R, Luth T, Muhling J, Hassfeld S. Automated laser registration in image-guided
540 surgery: evaluation of the correlation between laser scan resolution and navigation accuracy.
541 *International journal of oral and maxillofacial surgery*. 2004;33(7):642-8.
- 542 14. Koo S, Gold GE, Andriacchi TP. Considerations in measuring cartilage thickness using
543 MRI: factors influencing reproducibility and accuracy. *Osteoarthritis and cartilage / OARS,*
544 *Osteoarthritis Research Society*. 2005;13(9):782-9.
- 545 15. Trinh N, Lester J, Fleming B, Tung G, Kimia B. Accurate Measurement of Cartilage
546 Morphology Using a 3D Laser Scanner. In: Beichel R, Sonka M, editors. *Computer Vision*
547 *Approaches to Medical Image Analysis*. Lecture Notes in Computer Science. 4241: Springer
548 Berlin Heidelberg; 2006. p. 37-48.

- 549 16. Bowers ME, Trinh N, Tung GA, Crisco JJ, Kimia BB, Fleming BC. Quantitative MR
550 imaging using "LiveWire" to measure tibiofemoral articular cartilage thickness. Osteoarthritis and
551 cartilage / OARS, Osteoarthritis Research Society. 2008;16(10):1167-73.
- 552 17. Thiruvengkatachari B, Al-Abdallah M, Akram NC, Sandler J, O'Brien K. Measuring 3-
553 dimensional tooth movement with a 3-dimensional surface laser scanner. American journal of
554 orthodontics and dentofacial orthopedics : official publication of the American Association of
555 Orthodontists, its constituent societies, and the American Board of Orthodontics.
556 2009;135(4):480-5.
- 557 18. Geomagic. Qualify 2012 2011 [cited 2014 10 May]. Available from:
558 [http://dl.geomagic.com/media/marketing/2012_Brochures/MASTER-](http://dl.geomagic.com/media/marketing/2012_Brochures/MASTER-12_29_11_QQP_A4_English_eVersion.pdf)
559 [12_29_11_QQP_A4_English_eVersion.pdf](http://dl.geomagic.com/media/marketing/2012_Brochures/MASTER-12_29_11_QQP_A4_English_eVersion.pdf).
- 560 19. Besl PJ, McKay ND. A method for registration of 3-D shapes. Pattern Analysis and
561 Machine Intelligence, IEEE Transactions on. 1992;14(2):239-56.
- 562 20. Audette MA, Ferrie FP, Peters TM. An algorithmic overview of surface registration
563 techniques for medical imaging. Medical image analysis. 2000;4(3):201-17.
- 564 21. Jansson T. Feature Based Registration. January; 2006.
- 565 22. Hebert M, Krotkov E, editors. 3-D measurements from imaging laser radars: how good are
566 they? Intelligent Robots and Systems '91 'Intelligence for Mechanical Systems, Proceedings IROS
567 '91 IEEE/RSJ International Workshop on; 1991 3-5 Nov 1991.
- 568 23. Huising EJ, Gomes Pereira LM. Errors and accuracy estimates of laser data acquired by
569 various laser scanning systems for topographic applications. ISPRS Journal of Photogrammetry
570 and Remote Sensing. 1998;53(5):245-61.
- 571 24. Bao J, Yao YL. Analysis and Prediction of Edge Effects in Laser Bending. Journal of
572 Manufacturing Science and Engineering. 2000;123(1):53-61.

- 573 25. Böhler W, Bordas Vicent M, Marbs A. Investigating Laser Scanner Accuracy-The
574 International Archives of Photogrammetry, Remote Sensing and Spatial Information Sciences,
575 Vol. XXXIV, Part. 2003;5:C15.
- 576 26. Zeibak R, Filin S. Managing uncertainty in the detection of changes from terrestrial laser
577 scanners data. XXI ISPRS Congress: Commission V, WG 3. Beijing2008.
- 578 27. Tang P, Akinci B, Huber D. Quantification of edge loss of laser scanned data at spatial
579 discontinuities. Automation in Construction. 2009;18(8):1070-83.
- 580 28. Sanz-Cortiella R, Llorens-Calveras J, Rosell-Polo JR, Gregorio-Lopez E, Palacin-Roca J.
581 Characterisation of the LMS200 laser beam under the influence of blockage surfaces. Influence
582 on 3D scanning of tree orchards. Sensors (Basel, Switzerland). 2011;11(3):2751-72.
- 583 29. Loftus G. On interpretation of interactions. Memory & Cognition. 1978;6(3):312-9.
- 584 30. Newman I, Newman C. Conceptual statistics for beginners. 2 ed. Lanham, MD: University
585 Press of America; 1994.
- 586 31. Stevens. Interaction effects in ANOVA 2004 [cited 2015 3 January]. Available from:
587 <http://pages.uoregon.edu/stevensj/interaction.pdf>.
- 588 32. Andrew DP, Pedersen PM, McEvoy CD. Research methods and design in sport
589 management: Human Kinetics; 2011.
- 590 33. Moss JP, Linney AD, Grindrod SR, Moss CA. A Laser Scanning System for the
591 Measurement of Facial Surface Morphology. Optics and Lasers in Engineering. 1989, 10:179-190
- 592 34. Motohashi N, Kurdoa T. A 3D computer-aided design system applied to diagnosis and
593 treatment planning in orthodontics and orthognathic surgery. European Journal of Orthodontics.
594 1999, 21:263-274
- 595 35. Bell A, Ayoub AF, Siebert P. Assessment of the accuracy of three-dimensional imaging
596 system for archiving study models. Journal of orthodontics. 2003, 30:219-223

- 597 36. Zilberman O, Huggare JV, Parikakis KA . Evaluation of the Validity of Tooth Size and
598 Arch Width Measurements Using Conventional and Three-dimensional Virtual Orthodontic
599 Models. *The Angle Orthodontist*. 2003, 73(3):301-306
- 600 37. Winder RJ, Darvannb TA, McKnightc W, Mageed JDM, Ramsay-Baggs P. Technical
601 validation of the Di3D stereophotogrammetry surface imaging system. *British Journal of Oral and*
602 *Maxillofacial Surgery*. 2008, 46:33-37
- 603 38. Nouri M, Massudi R, Bagheban AA, Azimi S, Fereidooni . The accuracy of a 3-D laser
604 scanner for crown width measurements. *Aust Orthod J*. 2009, 25(1):41-47
- 605 39. Fleming PS, Marinho V, Johal A , Orthodontic measurements on digital study models
606 compared with plaster models: a systematic review. *Orthodontics & Craniofacial Research*. 2001,
607 14(1):1-16
- 608 40. El-Katatny I, Masood SH, Morsi YS. Error analysis of FDM fabricated medical replicas.
609 *Rapid Prototyping Journal*. 2010, 16(1):36-43
- 610 41. Macario Alex. Editorial, What does one minute of operating room time cost? *Journal of*
611 *Clinical Anesthesia*. 2010. 22: 233-236
- 612
- 613

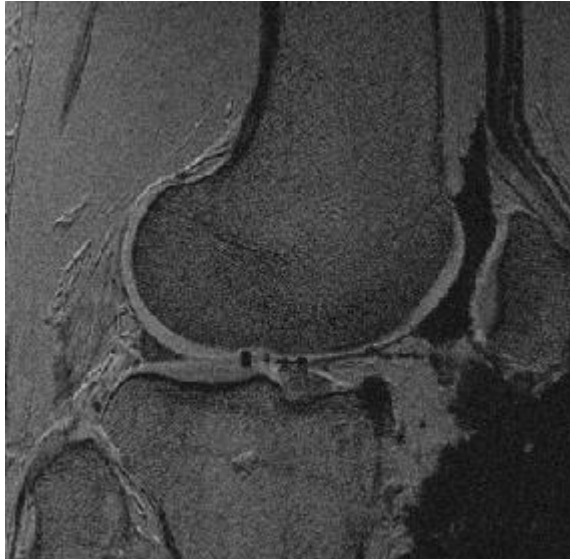


Figure 1: A sample MRI scan of the right knee joint

614

615

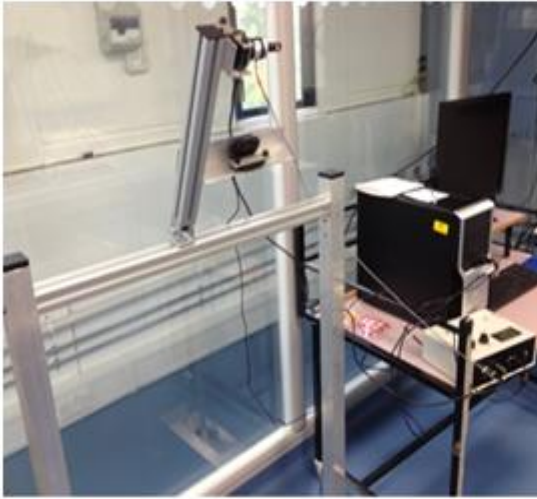
616

617

618

619

620



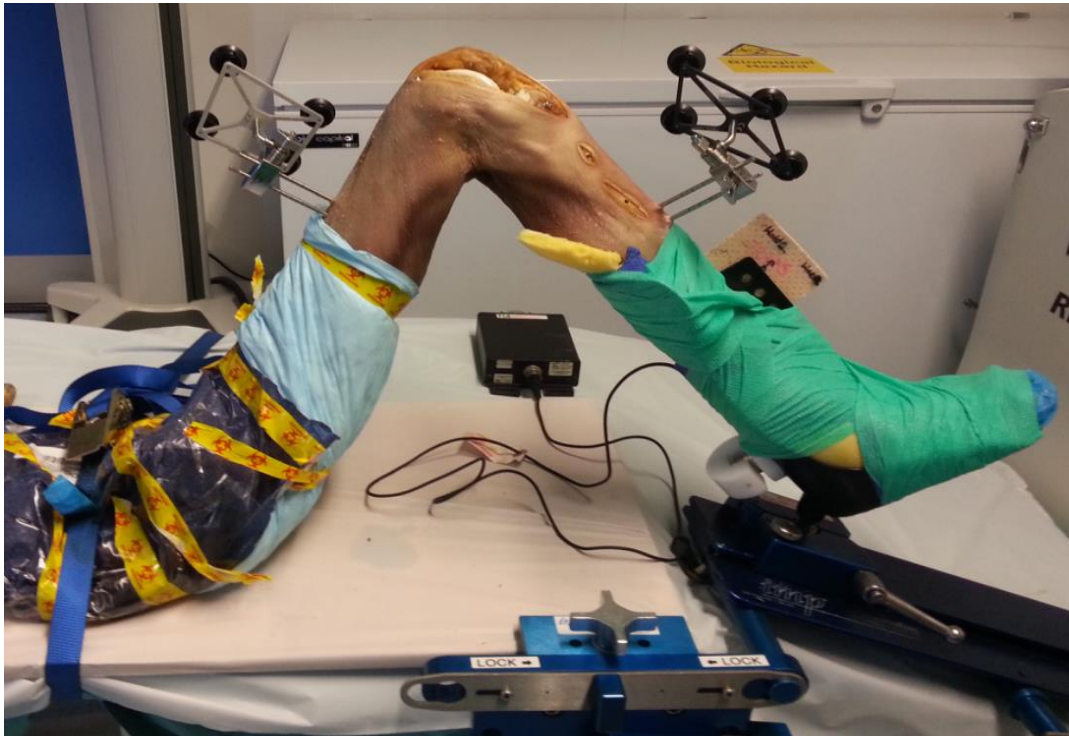
(a)



(b)

621 Figure 2: 3D Laser scanner (a): Scanner mounted on the aluminium extrusion framework (b):
622 Laser scanner mounted on the joint six of the MAKO RIO® arm
623

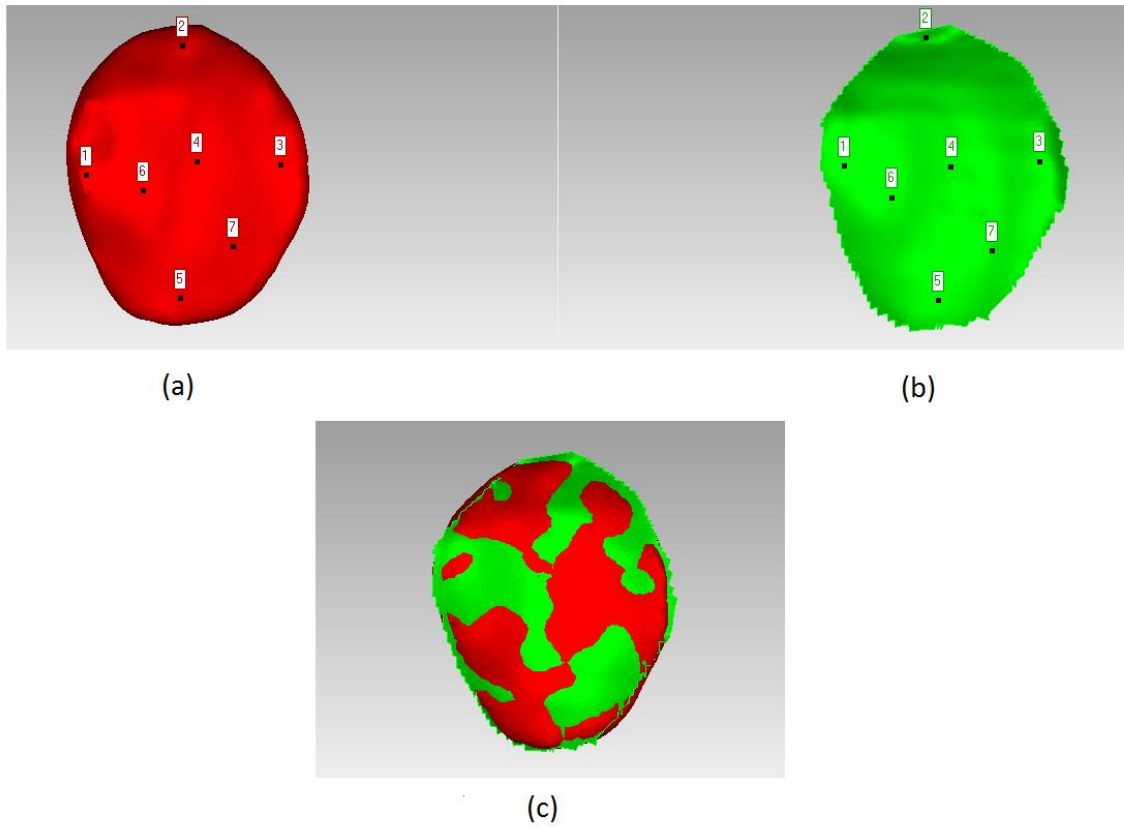
624



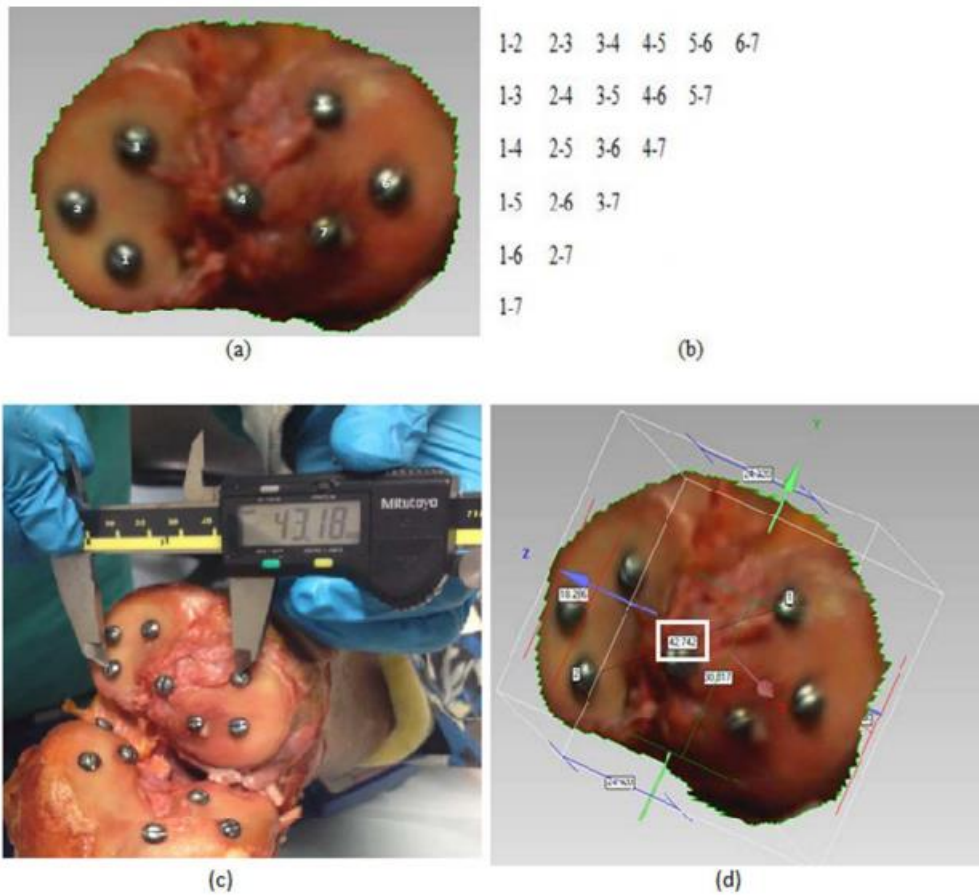
625

626 Figure 3: Sample cadaver set up on the bed with the attached arrays for MAKO registration

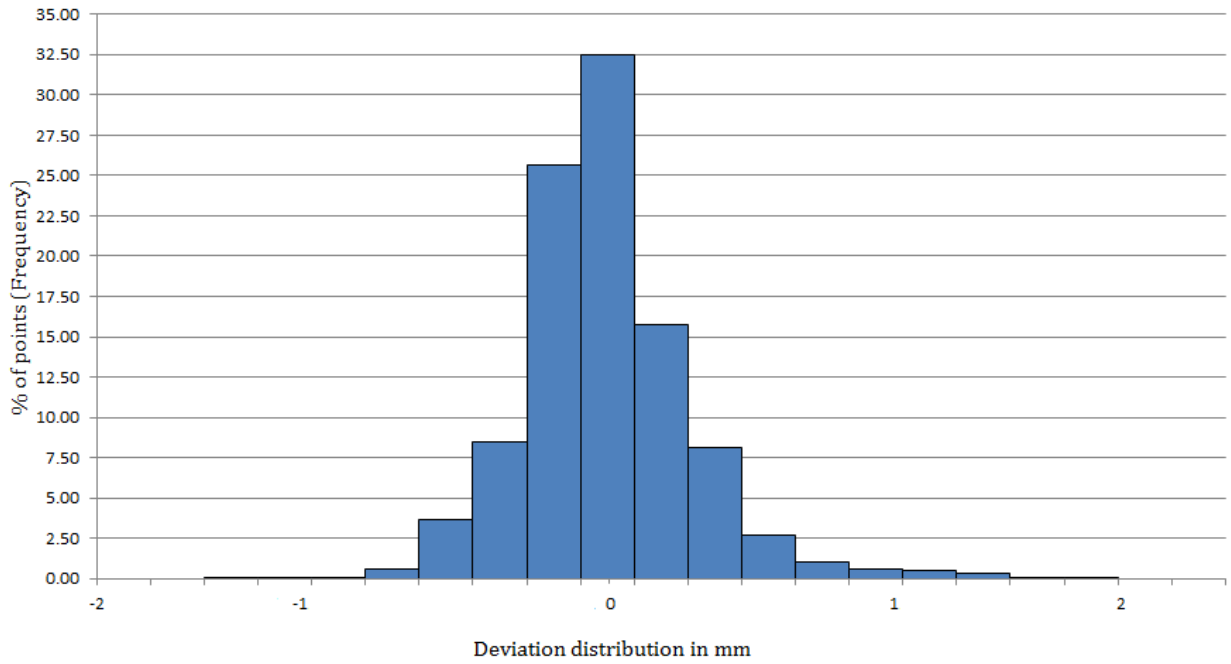
627



628 Figure 4: Manual registration by selecting random points over the left lateral tibial surface
629 (a): MRI generated 3D model (red) of the articular cartilage, set as a reference model. (b):
630 Corresponding 3D laser scan (green) of the same cartilage acquired intra-operatively, set as a test
631 model. (c): Rough manual registration between two surfaces
632

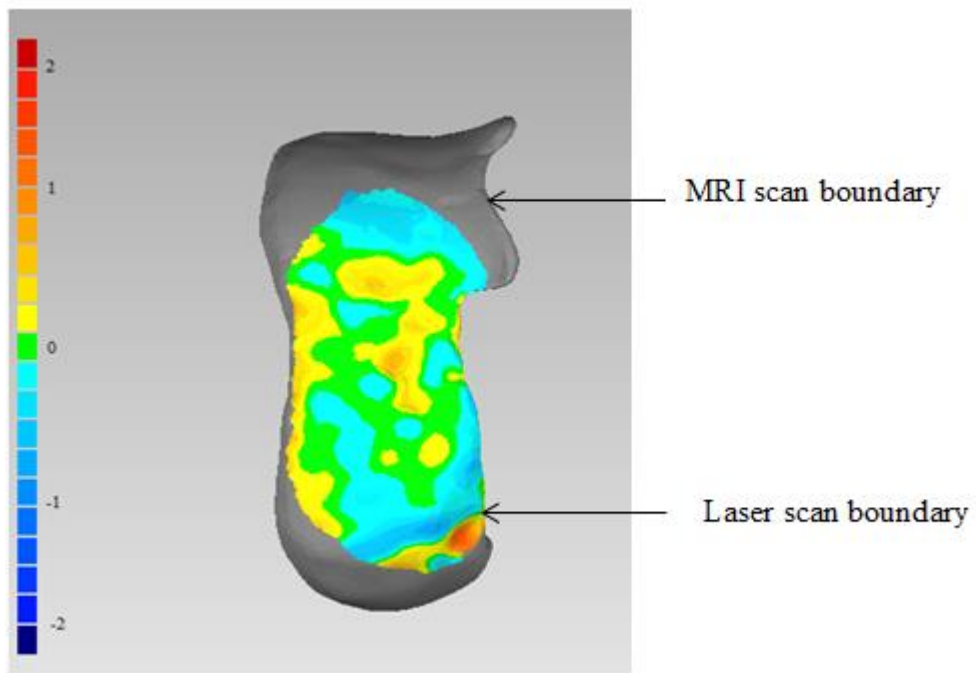


633 Figure 5: Distance measurements between the screw markers on the tibial condyle
 634 (a): Placement of seven screws over the surface (b): Total number of measurements (21)
 635 computed between every pair of the points (c): Direct distance measurement acquired using
 636 digital vernier calliper (d): Distance measurement (in the white box) acquired on the
 637 corresponding digitised 3D laser scan and formulated using Geomagic Qualify®
 638



639
 640 Figure 6: Deviation distribution between MRI and laser scan of an example right femoral lateral
 641 cartilage

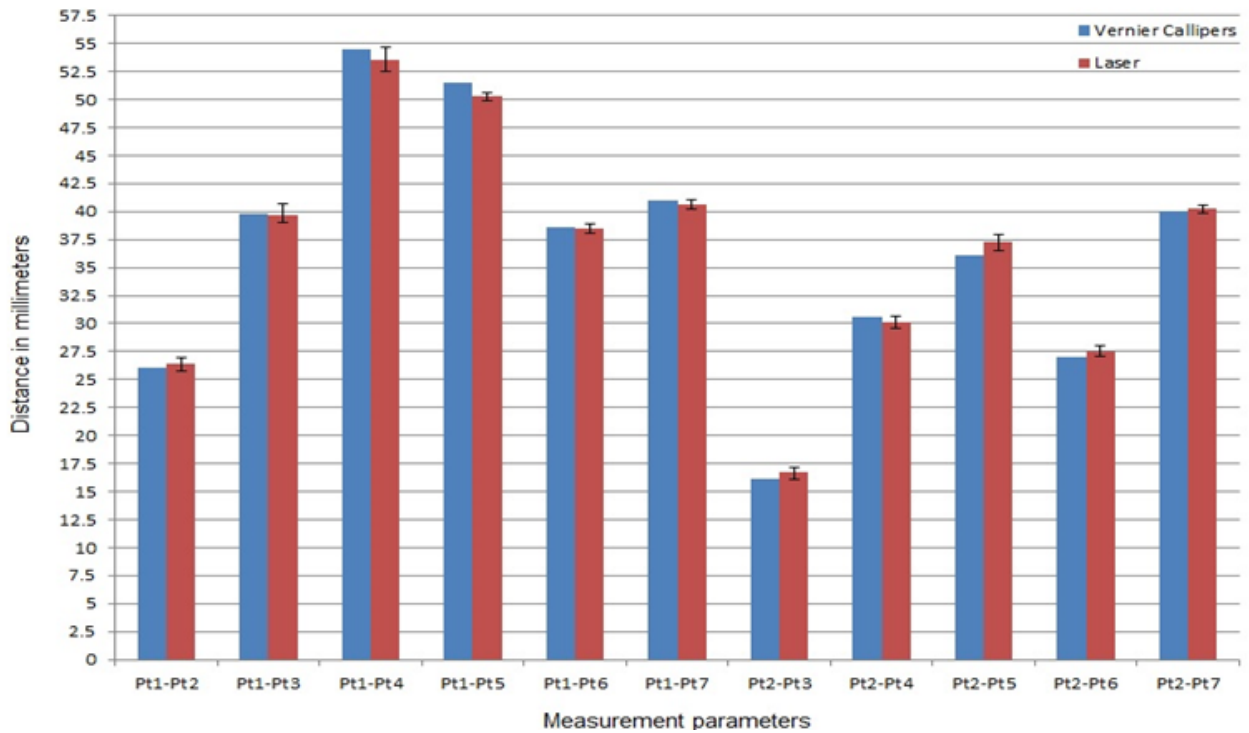
642 Deviation in mm is plotted against the percentage of points within the range of deviations. Note:
 643 $\pm d_{\max}$ occurred at the periphery
 644



645 Figure 7: Top view of the colour deviation map showing spatial distribution of the deviations
 646 between MRI and laser scan of right femoral lateral cartilage

647 The posterior and superior condylar region is clipped as the laser scan was acquired with a
 648 minimal exposure (90 mm, mimicking UKA). Note: Large errors ($\pm d_{\max}$) at the periphery

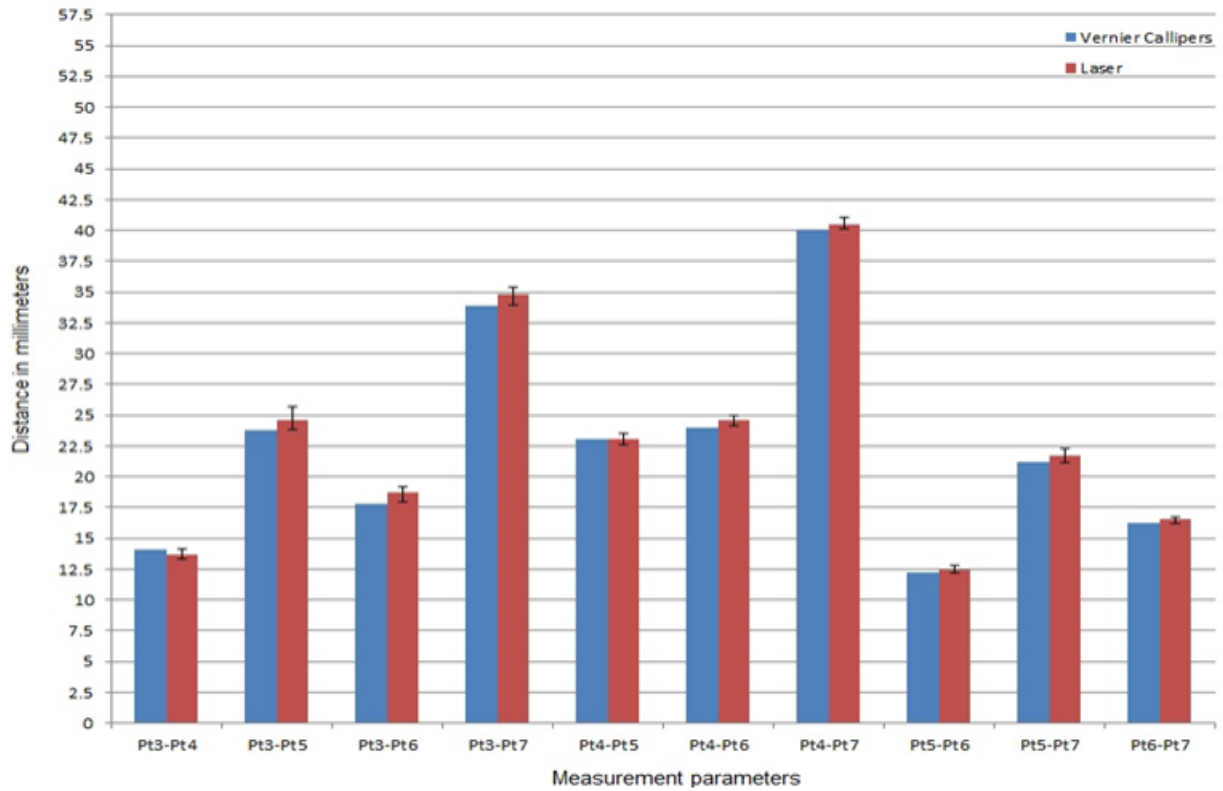
649



650 Figure 8: Bar graph for the comparison for the distance calculations between vernier calliper and
 651 3D laser scans

652 (a): Bar graph for first 11 pairs of screws. (b): Bar graph for remaining 10 pairs of screws

653 Note: Blue bar is the measurement recorded by the vernier calliper, whereas red bar is the mean
 654 value of the measurements on the laser scans. Error bars indicate the range of values (minimum
 655 and maximum values). All the measurement differences between vernier calliper and laser were
 656 statistically not significant; $P > 0.05$



657 Figure 8: Bar graph for the comparison for the distance calculations between vernier calliper and
 658 3D laser scans

659 (a): Bar graph for first 11 pairs of screws. (b): Bar graph for remaining 10 pairs of screws

660 Note: Blue bar is the measurement recorded by the vernier calliper, whereas red bar is the mean
 661 value of the measurements on the laser scans. Error bars indicate the range of values (minimum
 662 and maximum values). All the measurement differences between vernier calliper and laser were
 663 statistically not significant; $P > 0.05$